COMPDYN 2011
3rd ECCOMAS Thematic Conference on
Computational Methods in Structural Dynamics and Earthquake Engineering
M. Papadrakakis, M. Fragiadakis, V. Plevris (eds.)
Corfu, Greece, 25-28 May 2011

ACCURATE NUMERICAL SOLUTIONS OF STRUCTURAL DYNAMICS AND WAVE PROPAGATION PROBLEMS BASED ON NEW DISPERSION-REDUCTION TECHNIQUE AND NEW TWO-STAGE TIME-INTEGRATION TECHNIQUE

A. Idesman

Texas Tech University
Box 41021, Lubbock, TX 79409, USA
e-mail: alexander.idesman@coe.ttu.edu

Keywords: time integration, spurious oscillations, numerical dispersion

Abstract. *There are the following issues with existing numerical methods for elastodynamics problems (including wave propagation and structural dynamics problems): a) a large dispersion error of space-discretization methods may lead to a great error in space, especially in the 2-D and 3-D cases; b) due to spurious high-frequency oscillations, the lack of reliable numerical techniques that yield an accurate solution of wave propagation in solids; c) the treatment of the error accumulation for long-term integration; d) the selection of an effective time-integration method among known ones; e) the selection of the size of a time increment for a time-integration method with numerical dissipation; f) the increase in accuracy and the reduction of computation time for real-world dynamic problems. A new numerical approach for computer simulation of the dynamic response of linear elastic structures is suggested, resolves the issues listed and includes two main components: a) a new dispersion reduction technique for linear finite elements based on the extension of the modified integration rule method to elastodynamics problems, and b) a new two-stage time-integration technique with the filtering stage. The suggested two-stage time-integration technique includes the stage of basic computations and the filtering stage, new first-, second- and high-order accurate time-integration methods for elastodynamics, and a new calibration procedure for the selection of the minimum necessary amount of numerical dissipation for time-integration methods, new criteria for the selection of time-integration methods for elastodynamics. In contrast to existing approaches, the new technique does not require guesswork for the selection of numerical dissipation and does not require interaction between users and computer codes for the suppression of spurious high-frequency oscillations. Different discretization methods in space such as the finite element method, the spectral element method, the boundary element method, and others can be used with the suggested two-stage time-integration approach. 1-D and 3-D numerical examples show that the new approach used with the finite element method yields an accurate non-oscillatory solution for impact and wave propagation problems and considerably reduces the number of degrees of freedom and the computation time in comparison with existing methods.*

1 INTRODUCTION

The application of finite elements in space to transient acoustics or transient linear elastodynamics problems leads to a system of ordinary differential equations in time

$$\mathbf{M}\,\ddot{\mathbf{U}} + \mathbf{C}\,\dot{\mathbf{U}} + \mathbf{K}\,\mathbf{U} = \mathbf{R}, \tag{1}$$

where $\mathbf{M}$, $\mathbf{C}$, $\mathbf{K}$ are the mass, damping, and stiffness matrices, respectively, $\mathbf{U}$ is the vector of the nodal displacement, $\mathbf{R}$ is the vector of the nodal load. The case of zero natural viscosity, $\mathbf{C} = \mathbf{0}$, is considered in the paper. It is known that even the exact solution to Eq. (1) contains the numerical dispersion error, which is also related to the space discretization error; e.g., see [1, 2, 3, 4, 5, 6, 7, 8, 9, 10] and others. The decrease in the space discretization error by the use of mesh refinement considerably increases computational costs. Therefore, several techniques have been proposed for the reduction in the numerical dispersion error. One simple approach for acoustic and elastic wave propagation problems is based on the use of the averaged mass matrix in Eq. (1) instead of the consistent or lumped mass matrix $\mathbf{M}$; see [5, 6, 7, 8] and others. For linear finite elements, this technique reduces the relative error in the wave velocity for harmonic waves from the second order to the fourth order of accuracy in the 1-D case. However, these results are not valid in the general case of harmonic wave propagation for 2-D and 3-D problems (nevertheless, in the 2-D and 3-D cases, the averaged mass matrix yields more accurate results compared with the standard mass matrix). Another simple technique for linear finite elements, which is suggested in [9] for acoustic waves in the 2-D case, is based on the modified integration rule for the mass and stiffness matrices. In contrast to the averaged mass matrix, this approach increases the accuracy for the phase velocity from the second order to the fourth order in the general multi-dimensional case of acoustic waves. However, the applicability of the modified integration rule to linear elastodynamics problems has not been studied.

As we mentioned above, the analysis of numerical dispersion is based on propagation of harmonic waves. In the general case of loading (boundary conditions), the numerical study of the effectiveness of the finite element formulations with the reduced dispersion error is difficult due to the presence of spurious high-frequency oscillations in numerical solutions; e.g., see [3, 5].

In the current paper, we will apply two dispersion reduction techniques for linear finite elements to 1-D and 3-D impact problems. Similar to the classical finite element technique for elastodynamics, the finite element formulations with reduced dispersion also suffer spurious high-frequency oscillations in numerical solutions (e.g., see below). Therefore, for obtaining accurate numerical results and for the numerical study of the effectiveness of the dispersion reduction techniques applied to elastodynamics problems with general loading, the two-stage time-integration technique with the filtering stage (developed in our previous papers [11, 12, 13]) is used along with the finite elements with reduced dispersion. This technique identifies and removes spurious high-frequency oscillations from numerical solutions. 1-D and 3-D impact problems for which all frequencies of the semi-discrete system, Eq. (1), are excited are solved with the standard and new techniques. Numerical results show that compared with the standard mass and stiffness matrices, the simple dispersion reduction techniques lead to a considerable reduction in the number of degrees of freedom and computation time at the same accuracy, especially for multi-dimensional problems.

2 NUMERICAL TECHNIQUE

2.1 Dispersion reduction of linear finite elements (see [14])

We will use two numerical techniques which reduce the dispersion error of linear finite elements at the space discretization. The first approach is based on the use of the mass matrix $\boldsymbol{M}$ calculated as a weighted average of consistent and lumped mass matrices with the weighting factor γ (similar to that used in [5, 6, 8])

$$\boldsymbol{M} \,=\, \boldsymbol{M}^{lump}\gamma + \boldsymbol{M}^{cons}(1-\gamma) \tag{2}$$

where γ is the parameter to be determined. The second technique is the extension of the modified integration rule to the case of elastodynamics suggested in our paper [14]. For the dispersion reduction of linear finite elements, the mass and stiffness matrices of each finite element are calculated with the modified integration rule (similar to those used in [9])

$$\boldsymbol{M}^e \,=\, \int\limits_{-1}^{1} \boldsymbol{N}^T(s)\boldsymbol{N}(s)det(\boldsymbol{J})ds \approx \sum_{i=1}^{2} \boldsymbol{N}^T((-1)^i\alpha_M)\,\boldsymbol{N}((-1)^i\alpha_M)det(\boldsymbol{J})\,, \tag{3}$$

$$\boldsymbol{K}^e \,=\, \int\limits_{-1}^{1} E\boldsymbol{B}^T(s)\boldsymbol{B}(s)det(\boldsymbol{J})ds \approx \sum_{i=1}^{2} E\boldsymbol{B}^T((-1)^i\alpha_K)\,\boldsymbol{B}((-1)^i\alpha_K)det(\boldsymbol{J}) \tag{4}$$

in the 1-D case,

$$\boldsymbol{M}^e \,=\, \int\limits_{-1}^{1}\int\limits_{-1}^{1}\int\limits_{-1}^{1} \boldsymbol{N}^T(s,t,q)\boldsymbol{N}(s,t,q)det(\boldsymbol{J})dsdtdq$$

$$\approx \sum_{i=1}^{2}\sum_{j=1}^{2}\sum_{p=1}^{2} \boldsymbol{N}^T((-1)^i\alpha_M,(-1)^j\alpha_M,(-1)^p\alpha_M)\,\boldsymbol{N}((-1)^i\alpha_M,(-1)^j\alpha_M,(-1)^p\alpha_M)det(\boldsymbol{J})\,, \tag{5}$$

$$\boldsymbol{K}^e \,=\, \int\limits_{-1}^{1}\int\limits_{-1}^{1}\int\limits_{-1}^{1} \boldsymbol{B}^T(s,t,q)\boldsymbol{D}\boldsymbol{B}(s,t,q)det(\boldsymbol{J})dsdtdq$$

$$\approx \sum_{i=1}^{2}\sum_{j=1}^{2}\sum_{p=1}^{2} \boldsymbol{B}^T((-1)^i\alpha_K,(-1)^j\alpha_K,(-1)^p\alpha_K)\,\boldsymbol{D}\boldsymbol{B}((-1)^i\alpha_K,(-1)^j\alpha_K,(-1)^p\alpha_K)det(\boldsymbol{J}) \tag{6}$$

in the 3-D case. Here, $\boldsymbol{N}$ and $\boldsymbol{B}$ are the standard finite element shape and B matrices; $\boldsymbol{D}$ is the matrix of elastic coefficients; $\boldsymbol{J}$ is the Jacobian matrix ($det(\boldsymbol{J}) = dx/2;\ dx^2/4;\ dx^3/8$ in the 1-D case, in the 2-D case for square elements and in the 3-D case for cubic elements, respectively; dx is the length of a finite element); E is Young's modulus; s, t, q are the isoparametric coordinates; α_M and α_K are the coordinates of the integration points for the mass and stiffness matrices to be determined (2 and $2 \times 2 \times 2 = 8$ integration points are used for linear elements in the 1-D and 3-D cases, respectively); e.g., see [15] for the derivation of finite element matrices. The integration error related to the application of the modified integration rule for the mass and stiffness matrices does not change the convergence rate of finite element solutions; see [9].

The analytical study of numerical dispersion shows (see our paper [14]) that the use of the averaged mass matrix with $\gamma = 0.5$ increases the accuracy in the calculation of the wave velocity from the second order to the fourth order in the 1-D case. Completely equivalent results for the numerical dispersion reduction are obtained with the modified integration rule in the 1-D case

with $\alpha_M = \sqrt{\frac{2}{3}}$. However, in the multi-dimensional cases with the presence of compressional and shear waves, these results are valid only under some specific conditions. For example, for the averaged mass matrix ($\gamma = 0.5$), the increase in the order of accuracy for the phase velocity is valid only for the waves propagating along the coordinate axes of uniform meshes. The modified integration rule with $\alpha_M = \sqrt{\frac{2}{3}}$ and $\alpha_K = \sqrt{\frac{4(2\nu-1)}{3(4\nu-3)}}$ (ν is Poisson's ratios) additionally allows the extension of the results of the 1-D case only for the compressional waves or only for the shear waves propagating in any direction in the 2-D case and propagating in any direction within the coordinate planes of uniform meshes in the 3-D case.

2.2 The two-stage time-integration technique with filtering spurious oscillations (see [11, 12, 13])

The standard finite elements and the finite elements with reduced dispersion described in the previous section lead to the appearance of spurious high-frequency oscillations at time integration of Eq. (1) for wave propagation and impact problems. Below we briefly describe the approach developed in our previous papers [11, 12, 13] which, for the standard finite elements and for the finite elements with reduced dispersion, allows accurate numerical solutions of elastodynamics problems without spurious oscillations. It includes the two-stage time-integration technique with the stage of basic computations and the filtering stage, the implicit time-continuous Galerkin (TCG) method with large numerical dissipation and the calibration procedure for the selection of the minimum necessary amount of numerical dissipation (in terms of a time increment) for the implicit TCG method; see also the Appendix.

The idea of the two-stage time-integration technique is very simple. Because for linear elastodynamics problems there is no interaction between different modes during time integration (they are integrated independently of each other; e.g., see [12, 13]), the most accurate time-integration method (usually without numerical dissipation or artificial viscosity) should be used at the stage of basic computations, especially for a long-term integration. This means that all modes including high-frequency modes are integrated very accurately and the solution includes spurious high-frequency oscillations after basic computations. For the damping out of spurious high modes, a time-integration method with large numerical dissipation (or artificial viscosity) is used for a number of time increments for the filtering of spurious oscillations (the filtering stage). A small number of time increments for implicit time-integration methods is sufficient for the filtering stage, with negligible error accumulation at low modes (e.g., 10 time increments with the implicit TCG with large numerical dissipation is used with the proposed technique at the filtering stage for all elastodynamics problems; see [13]).

The main advantages of the developed approach are as follows. The suggested numerical technique: a) allows the selection of the best time-integration method for basic computations from simple criteria (the most important one being the accuracy of the method); b) includes pre-, or/and post-processing for filtering spurious high-frequency oscillations, which requires little computation time compared with that for the stage of basic computations (a small number of time increments with the implicit TCG method with large numerical dissipation is used for the filtering stage); c) yields no error accumulation due to numerical dissipation (or artificial viscosity) at the stage of basic computations; d) allows the calibration of spurious oscillations at different observation times (see [12, 13] and the Appendix below) and does not require any guesswork for the selection of numerical dissipation or artificial viscosity as do existing approaches. Thus, the approach can be easily incorporated in computer codes and does not require interaction with users for the suppression of spurious high-frequency oscillations.

Summarizing, in contrast to existing approaches with one time integration method, the described technique is based on the application two different time integration methods to Eq. (1): one method is used for accurate integration of a semi-discrete system at the stage of basic computations and allows spurious oscillations; another method is used for filtering spurious oscillations at the pre-, or/and post-processing stage. At mesh refinement, the numerical solutions obtained with the two-stage time-integration technique include more modes (because a finer mesh requires smaller numerical dissipation; see Eqs. (13)-(15) in the Appendix), exclude spurious high modes, and converge to exact solutions.

In the current paper, we will use the standard implicit trapezoidal rule with small time increments for basic computations in order to obtain an accurate solution of the semi-discrete elastodynamics problem, Eq. (1), with a negligible error in time (this solution contains spurious high-frequency oscillations). We should mention that other known implicit or explicit time-integration methods can also be used for basic computations with very small time increments (the trapezoidal rule is the most accurate second-order time-integration method). For filtering spurious oscillations, the implicit TCG method with large numerical dissipation developed in [12, 13] and briefly described in the Appendix is used at the filtering stage (the post-processing stage).

3 NUMERICAL MODELING

The new numerical approach is implemented into the finite element code FEAP [16]. 1-D and 3-D impact linear elastodynamics problems will be considered below. Due to spurious high-frequency oscillations, these problems cannot be accurately solved by existing time-integration methods based on the introduction of artificial viscosity (or numerical dissipation) at each time increment, especially in the case of long-term integration. For the filtering of spurious oscillations in the problems solved below, the filtering stage will be used with the TCG method with $N = 10$ time increments (5 positive plus 5 negative time increments) the size of which is calculated according to Eqs. (13) - (15) with $\Omega_{0.1}(N = 10) = 0.81$ (see [12, 13, 17] and the Appendix below).

3.1 1-D impact of an elastic bar against a rigid wall

First, the impact of an elastic bar of the length $L = 4$ against a rigid wall is considered in the 1-D case (see Fig. 1a). Young's modulus is chosen to be $E = 1$ and the density to be $\rho = 1$. The following boundary conditions are applied: the displacement $u(0, t) = t$ (which corresponds to the velocity $v(0, t) = v_0 = 1$) and $u(4, t) = 0$ (which corresponds to the velocity $v(4, t) = 0$). Initial displacements and velocities are zero; i.e., $u(x, 0) = v(x, 0) = 0$. The analytical solution to this problem includes the continuous variation of displacements $u_a(x, t) = t - x$ for $t \geq x$ and $u_a(x, t) = 0$ for $t \leq x$, and the piecewise continuous variation of velocities and stresses $v_a(x, t) = -\sigma^a(x, t) = 1$ for $t \geq x$ and $v_a(x, t) = \sigma^a(x, t) = 0$ for $t \leq x$ (at the interface $x = t$, jumps in stresses and velocities occur). The observation time is chosen to be $T = 18$. During this time the velocity pulse travels within the bar with two reflections from each end of the bar.

It is known that the application of traditional semi-discrete methods to this problem leads to oscillations in velocities and stresses due to the spurious high-frequency response [11, 18, 19]. As we will see (e.g., from Fig. 1b), finite elements with reduced numerical dispersion reduce these oscillations after basic computations but they do not completely remove them from the numerical solution. Therefore, the two-stage procedure with the filtering stage as described in

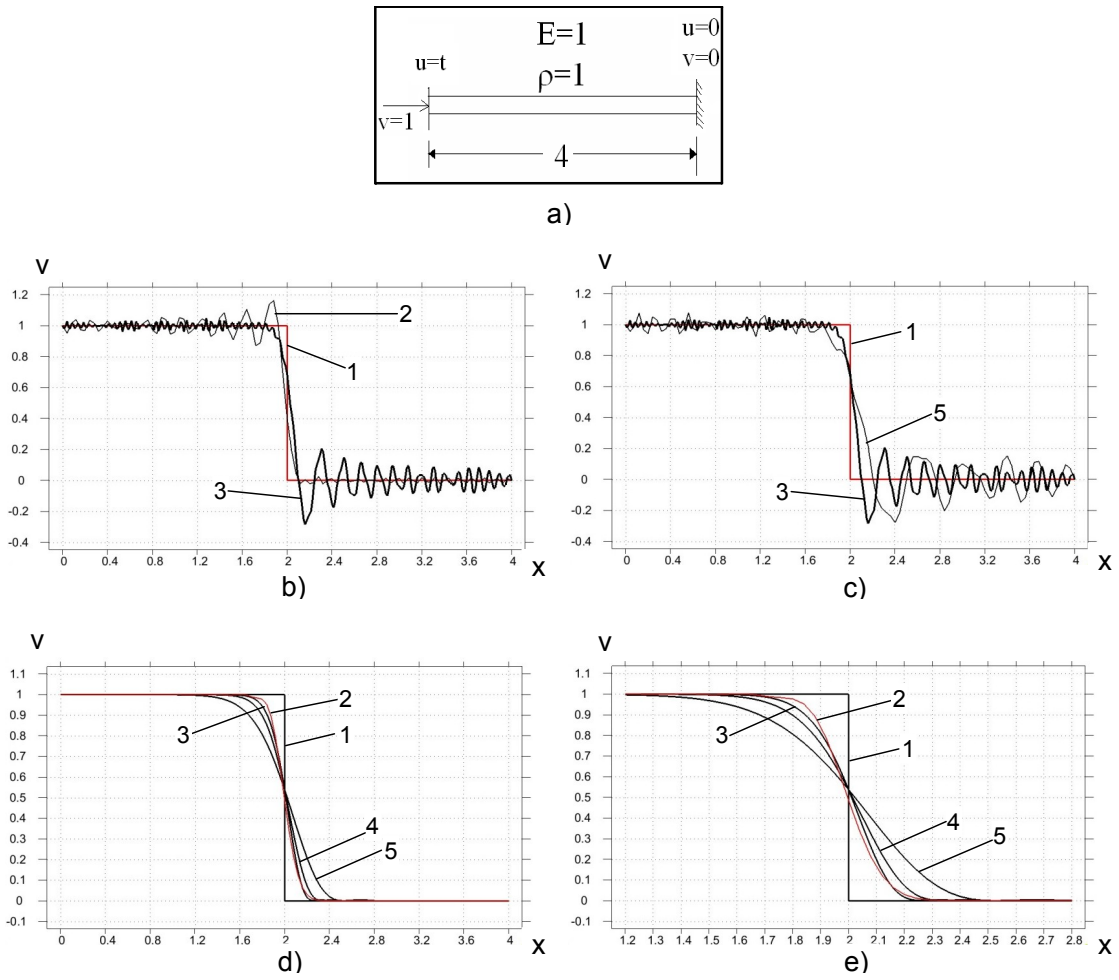

Figure 1: Impact of an elastic bar of length $L = 4$ against a rigid wall (a). Velocity distribution along the bar at observation time $T = 18$ after basic computations (b, c) and after post-processing (d, e). Curves 1 correspond to the analytical solution. Curves 2 correspond to the numerical solution with the averaged mass matrix ($\gamma = 0.5$) on a uniform mesh with 100 linear 2-node finite elements. Curves 3, 4, 5 correspond to the numerical solutions with the consistent mass matrix on uniform meshes with 300, 200 and 100 linear 2-node finite elements, respectively. e) shows the zoomed graph d) in the range $1.2 < x < 2.8$.

Section 2.2 will be applied for accurate and non-oscillatory solutions. The 1-D impact problem with propagating discontinuities in stresses and velocities can be considered a good benchmark problem for the testing of new numerical methods for wave propagation problems.

The problem is solved on uniform meshes with 100, 200 and 300 $Q2$ linear finite elements with the consistent and averaged ($\gamma = 0.5$) mass matrices as well as on uniform meshes with 50 and 70 $Q3$ quadratic finite elements with the consistent mass matrix. We should mention that the techniques based on the modified integration rule with $\alpha_M = \sqrt{2/3}$ and the averaged mass matrix with $\gamma = 0.5$ are completely equivalent and yield the same results in the 1-D case. Because in the paper we study the improvement of the spatial accuracy due to the reduction in the numerical dispersion error, for the time integration of Eq. (1) at basic calculations we will use the trapezoidal rule with very small time increments $\Delta t = 0.001$. A further reduction of time increments does not practically affect the numerical results for the meshes used; i.e., the error in time is very small and can be neglected.

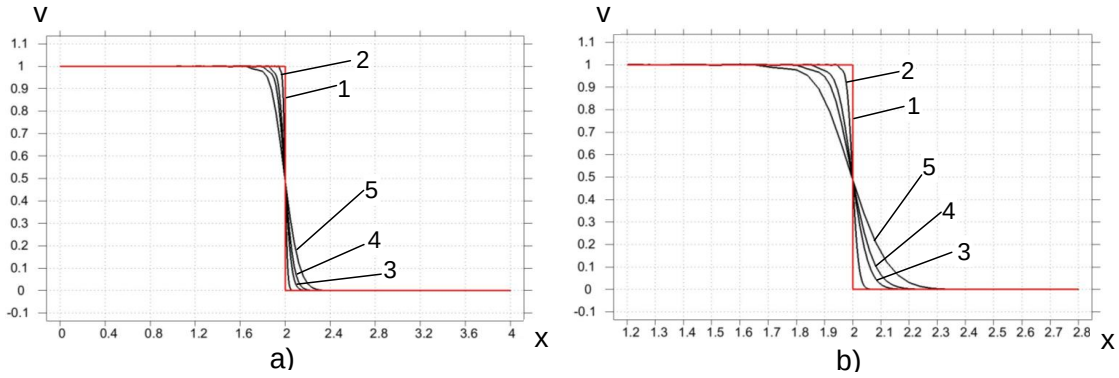

Figure 2: Velocity distribution along the bar at observation time $T = 18$ after post-processing. Curve 1 corresponds to the analytical solution. Curves 2, 3, 4, 5 correspond to the numerical solutions with the averaged mass matrix ($\gamma = 0.5$) on uniform meshes with 1000, 300, 200 and 100 linear 2-node finite elements, respectively. b) shows the zoomed graph a) in the range $1.2 < x < 2.8$.

Fig. 1 shows the numerical results for linear elements obtained with the consistent and averaged mass matrices after basic computations and after the filtering stage (post-processing). The use of the formulation with the reduced dispersion error reduces the amplitudes of spurious oscillations (see curve 2 in Fig. 1b) and yields a more accurate slope of the wave front at $x = 2$ (see curve 2 in Fig. 1b and curve 5 in Fig. 1c for the consistent mass matrix obtained at the same numbers of elements). However, the presence of spurious high-frequency oscillations makes it difficult to compare numerical results. After the filtering of spurious oscillations, we can see that for the selected observation time and at the same accuracy, the use of the averaged mass matrix reduces the number of degrees of freedom by a factor of three as compared with the case with the standard consistent mass matrix (see curves 2 and 3 in Fig. 1d,e). We should also mention that after basic computations the slopes of the wave front in the numerical solutions obtained on a uniform mesh with 100 elements and the averaged mass matrix and obtained on a uniform mesh with 300 elements and the consistent mass matrix are approximately the same (see curves 2 and 3 in Fig. 1b). After the filtering stage, the numerical results obtained with the averaged mass matrix converge to the analytical solution at mesh refinement; see Fig. 2. These numerical results for the 1-D impact problem after the filtering stage are similar to those obtained in [18] by the use of special non-linear discontinuity-capturing operators.

Fig. 3 shows that for the standard mass and stiffness matrices, quadratic finite elements yield more accurate results than linear finite elements (e.g., compare curves 4 and 5 obtained on the meshes with the same numbers of degrees of freedom). However, at the same numbers of degrees of freedom, the linear elements with the averaged mass matrix (or the modified integration rule) are more accurate than the quadratic elements with the consistent mass matrix (e.g., compare curves 2 and 4 in Fig. 3 obtained on the meshes with the same numbers of degrees of freedom). The comparison of curves 2 and 3 in Fig. 3 also shows that for the selected observation time and at the same accuracy, the linear elements with the reduced dispersion error reduces the number of degrees of freedom by a factor of 1.4 as compared with the case of the quadratic elements with the consistent mass matrix. In addition to this advantage, numerical solutions with linear elements require less computation time compared with that for quadratic elements because at the same numbers of degrees of freedom, the bandwidth of the mass and stiffness matrices for quadratic elements is twice of that for linear elements.

Remark. It is interesting to note that the range of frequencies in numerical solutions after

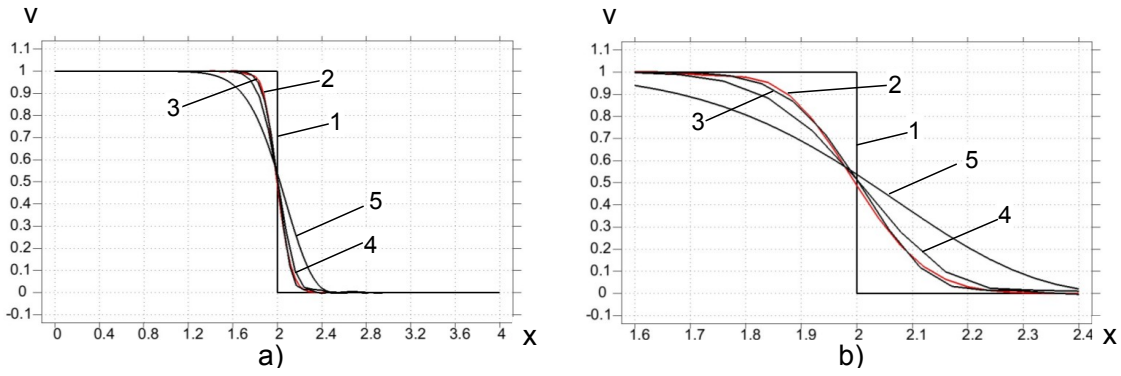

Figure 3: Velocity distribution along the bar at observation time $T = 18$ after post-processing. Curve 1 corresponds to the analytical solution. Curves 2 and 5 correspond to the numerical solutions on a uniform mesh with 100 linear 2-node finite elements with the averaged mass matrix ($\gamma = 0.5$) and with the consistent mass matrix, respectively. Curves 3 and 4 correspond to the numerical solutions with the consistent mass matrix on uniform meshes with 70 and 50 quadratic 3-node finite elements, respectively. b) shows the zoomed graph a) in the range $1.6 < x < 2.4$.

the filtering stage is indirectly determined by the size of the time increments calculated by Eqs. (13) - (14) (see the Appendix). The numerical results show that if the time increments calculated according to Eqs. (13) - (14) for the filtering stage are close to each other for the formulations with the consistent and averaged mass matrices on different uniform meshes, then the numerical solutions obtained on these different uniform meshes are close to each other. This means that Eqs. (13) - (14) allow the quantitative estimation of the advantage of the averaged mass matrix ($\gamma = 0.5$) compared with the consistent mass matrix. For example, for a uniform mesh with 100 linear finite elements and the averaged mass matrix ($\gamma = 0.5$), the size of the time increments at the filtering stage is $\Delta t_1 = 0.03447$ according to Eqs. (13) - (14). For a uniform mesh with 300 linear finite elements and the consistent mass matrix, the size of the time increments at the filtering stage is $\Delta t_2 = 0.03908$ according to Eqs. (13) - (14). Because Δt_2 is close to Δt_1, then curves 2 and 3 in Fig. 1d,e are close to each other (curve 2 is slightly more accurate because Δt_1 is slightly smaller than Δt_2); see also the analytical solution, curve 1. For a uniform mesh with 70 $Q3$ quadratic elements and the consistent mass matrix, the size of the time increments at the filtering stage is $\Delta t_3 = 0.03465$ according to Eqs. (13) - (14). Because Δt_3 is close to Δt_1, then curves 2 and 3 in Fig. 3 are close to each other.

3.2 3-D impact of an elastic bar against a rigid wall

A solid 3-D bar of length $L = 2$ with a square cross section $a \times a$ ($a = 2$) under impact loading at the left end $ACEM$ is considered; see Fig. 4. Due to symmetry, the problem is solved for a quarter of the bar $ACEMNFDB$ where planes $ABDC$ and $ABNM$ are the planes of symmetry. Young's modulus is chosen to be $E = 1$, Poisson's ratio to be $\nu = 0.3$, and the density to be $\rho = 1$. The following boundary conditions are applied: along the left end $ACEM$: $u_n = t$ (which corresponds to the instantaneous application of velocity $v_{load}(t) = v_0 = 1$) and $\tau_n = 0$; along planes $BDFN$, $CDEF$ and $EFNM$: $\sigma_n = 0$ and $\tau_n = 0$ (free surfaces); along planes $ABDC$, $ABNM$: $u_n = 0$ and $\tau_n = 0$ where u_n, v_n, and σ_n are the normal displacements, velocities and the tractive forces, respectively; τ_n are the tangential tractive forces. The observation time is chosen to be $T = 7$. During this time the velocity pulse travels within the bar with multiple reflections from the ends of the bar and from the external surfaces $CDFE$ and $EFNM$. We should mention that with the dimensionless coordinates $\tilde{x}$,

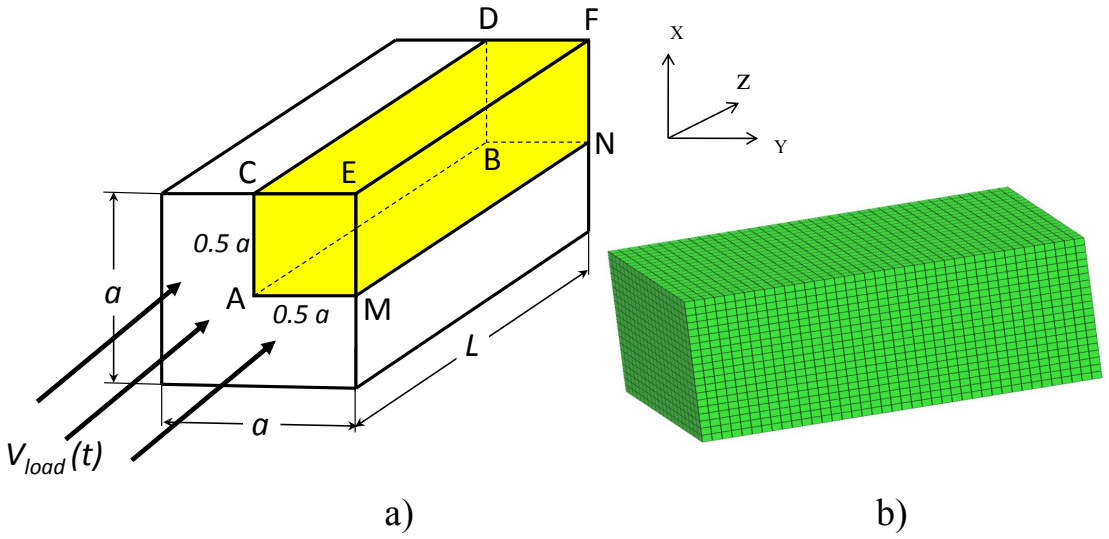

Figure 4: Impact of an elastic 3-D square bar of length $L = 2$ and width $a = 2$ against a rigid wall (a). A uniform mesh with $20 \times 20 \times 40 = 16000$ linear $Q8$ finite elements (b).

$\tilde{y}$ and $\tilde{z}$ and the dimensionless time $\tilde{t}$

$$\tilde{x} = \frac{x}{a}, \qquad \tilde{y} = \frac{y}{a}, \qquad \tilde{z} = \frac{z}{a}, \qquad \tilde{t} = \frac{tc_0}{a},$$

and with the normalized displacements $\tilde{u}_i$, velocities $\tilde{v}_i$, stresses $\tilde{\sigma}_{ij}$ and strains $\tilde{\varepsilon}_{ij}$

$$\tilde{u}_i = \frac{u_i c_0}{a v_0}, \qquad \tilde{v}_i = \frac{v_i}{v_0}, \qquad \tilde{\varepsilon}_{ij} = \frac{\varepsilon_{ij} c_0}{v_0},$$
$$\tilde{\sigma}_{ij} = \frac{\sigma_{ij} c_0 \sqrt{(1+\nu)(1-\nu)(1-2\nu)}}{\sqrt{2}\nu E v_0}, \qquad i,j = x,y,z$$

numerical results are independent of Young's modulus, the density, the amplitude of the velocity v_0 and the size a of a cross-section, and depend on Poisson's ratio ν and the dimensionless length of the bar L/a. Here, $c_0 = \sqrt{\frac{E}{\rho}}$ is the wave velocity in the 1-D case.

The problem is solved on uniform meshes with $10\times10\times20 = 2000$ and $20\times20\times40 = 16000$ linear quadrilateral $Q8$ elements with the modified integration rule for the mass and stiffness matrices ($\alpha_M = \sqrt{\frac{2}{3}}$ and $\alpha_K = \sqrt{\frac{4(2\nu-1)}{3(4\nu-3)}}$) as well as with the consistent and averaged ($\gamma = 0.5$) mass matrices. Similar to the 1-D impact problem, for the time integration of Eq. (1) at basic calculations we use the trapezoidal rule with very small time increments ($\Delta t = 0.001$). A further reduction of time increments does not practically affect the numerical results for the meshes used; i.e., the error in time is very small and can be neglected.

Figs. 5 and 6 show the distribution of the axial velocity along lines EF and AB at observation time $T = 7$. Similar to the previous 1-D impact problem, the numerical results after basic computations with the standard mass and stiffness matrices and the formulations with reduced numerical dispersion contain spurious oscillations; see Fig. 5. Fig. 6 shows the convergence of numerical results at mesh refinement after the filtering stage for the cases of the modified integration rule and the averaged mass matrix (these results do not contain spurious oscillations).

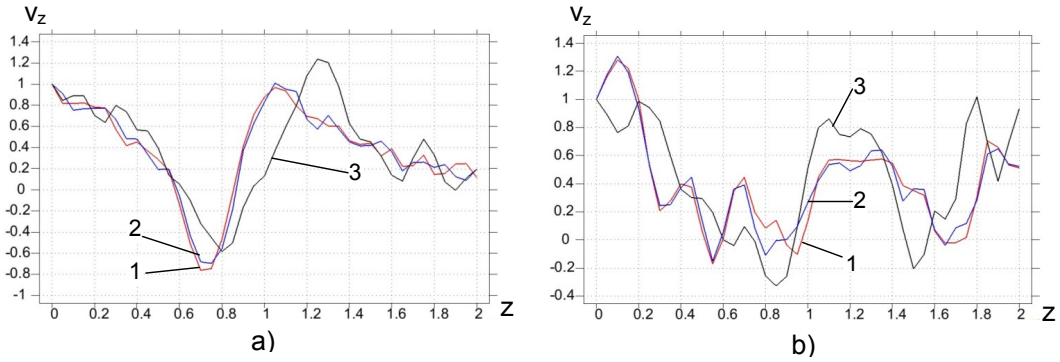

Figure 5: The distribution of the axial v_z (curves 1, 2, 3) velocity components along lines EF (a) and AB (b) (see Fig. 4) after basic computations at time $T = 7$ on a uniform mesh with $20 \times 20 \times 40 = 16000$ linear $Q8$ finite elements. The Poisson's ratios is $\nu = 0.3$. Curves 1, 2 and 3 correspond to the numerical solutions obtained by the use of the modified integration rule, the averaged mass matrix with $\gamma = 0.5$ and the consistent mass matrix, respectively.

The difference between the numerical results obtained with the modified integration rule and with the averaged mass matrix is small and can be neglected compared with the change in the numerical results at mesh refinement; see Fig. 6. Fig. 6 also shows that for the selected observation time $T = 7$, the use of the modified integration rule (or the averaged mass matrix) reduces the number of degrees of freedom by a factor of 8 (see curves 3, 4 and 5 in Fig. 6). Similar to the 1-D case, the size of the time increments at post-processing calculated by Eqs. (13) - (15) allows the quantitative estimation of the advantage of the modified integration rule (or the averaged mass matrix) compared with the consistent mass matrix. For example, for a uniform mesh with $10 \times 10 \times 20 = 2000$ finite elements and the modified integration rule (or the averaged mass matrix), the size of the time increments at the filtering stage is $\Delta t_1 = 0.084951$ according to Eqs. (13) - (15). For a uniform mesh with $20 \times 20 \times 40 = 16000$ finite elements and the consistent mass matrix, the size of the time increments at the filtering stage is $\Delta t_2 = 0.091410$ according to Eqs. (13) - (15). Because Δt_2 is close to Δt_1, then curves $3, 4$ and 5 in Fig. 6 are close to each other (curves $3, 4$ are slightly more accurate because Δt_1 is slightly smaller than Δt_2; see also curves 1 and 2 for the numerical solutions on a finer mesh).

4 CONCLUDING REMARKS

Two dispersion reduction techniques for linear finite elements has been applied to the to 1-D and 3-D impact problems, along with the filtering technique developed in our previous papers [11, 12, 13]. The considered finite element formulations with reduced numerical dispersion increase the accuracy of numerical solutions for elastodynamics problems; however, they do not remove all spurious high-frequency oscillations for wave propagation problems. These spurious oscillations make it difficult to estimate the effectiveness of the finite element formulations with reduced numerical dispersion applied to engineering elastodynamics problems. In the paper, this issue has been overcome by the use of the two-stage time-integration technique with the filtering stage [11, 12, 13], which identifies and removes spurious oscillations. Despite the fact that the modified integration rule yields a smaller numerical dispersion error compared with that for the averaged mass matrix, the numerical results after the filtering stage show that the difference between the numerical solutions obtained with the modified integration rule and with the averaged mass matrix is small and can be neglected compared with the change in

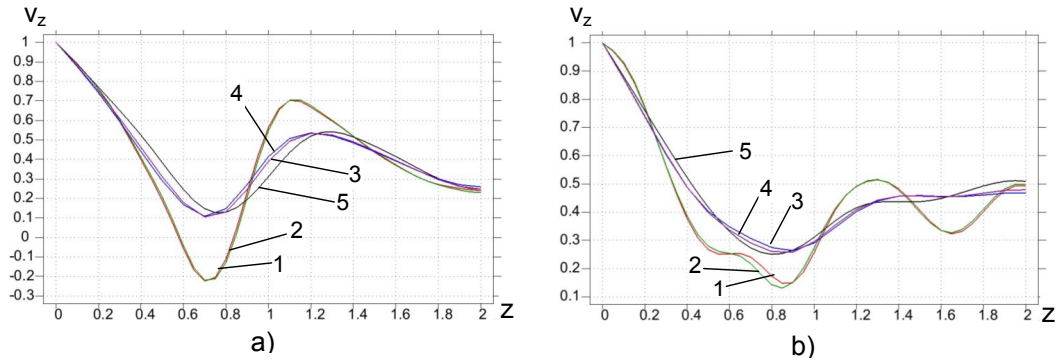

Figure 6: The distribution of the axial v_z (curves 1, 2, 3) velocity components along lines EF (a) and AB (b) (see Fig. 4) after post-processing at time $T = 7$. The Poisson's ratios is $\nu = 0.3$. Curves 1, 2, 5 and 3, 4 correspond to the numerical solutions on uniform meshes with $20 \times 20 \times 40 = 16000$ and $10 \times 10 \times 20 = 2000$ linear $Q8$ elements, respectively. The modified integration rule (curves 1 and 3), the averaged mass matrix with $\gamma = 0.5$ (curves 2 and 4) and the consistent mass matrix (curves 5) are used.

the numerical results at mesh refinement. The numerical results after the filtering stage also show that compared with the use of linear finite elements with the consistent mass matrix and the standard stiffness matrix, the finite element formulations with reduced numerical dispersion reduce the number of degrees of freedom for uniform meshes by a factor of $n = 2 \sim 3$ in the 1-D case and $n = 8 \sim 27$ in the 3-D case depending upon the material properties and the observation time. This leads to a huge reduction in computation time, especially for multi-dimensional elastodynamics problems. We should also mention that for the standard mass and stiffness matrices, quadratic finite elements yield more accurate results than linear elements; e.g., see [3, 13] and the numerical results in Section 3.1. However, the linear elements with reduced dispersion are more accurate than the quadratic elements with the standard mass and stiffness matrices. It is interesting to note that the range of frequencies in numerical solutions after the filtering stage is indirectly determined by the size of the time increments calculated by Eqs. (13) - (15) (see the Appendix). Numerical experiments show that if for uniform meshes with different numbers of degrees of freedom and with different types of finite elements, the time increments calculated according to Eqs. (13) - (15) are close to each other then the numerical solutions obtained on these meshes after the filtering stage are close to each other as well. This means that Eqs. (13) - (15) allow the quantitative estimation of the effectiveness of the finite element formulations with reduced numerical dispersion compared with the standard mass and stiffness matrices (the effectiveness is different for different observation times).

Acknowledgments

The research has been supported in part by the Air Force Research Lab, Eglin (contract # FA8651-08-D-0108) and by Texas Tech University.

Appendix. The implicit TCG method for filtering spurious high-frequency oscillations and the selection of the minimum necessary amount of numerical dissipation

Let us describe the implicit TCG method with large numerical dissipation suggested in [12, 13] that is used for the step-by-step time integration of the semi-discrete elastodynamics equations (1) at the filtering stage of the two-stage time-integration technique. The method is based on the linear approximations of displacements $U(t)$ and velocities $V(t)$ within a time

step Δt ($0 \le t \le \Delta t$)

$$\mathbf{U}(t) \,=\, \mathbf{U}_0 \,+\, \mathbf{U}_1\, t\,, \qquad \mathbf{V}(t) \,=\, \mathbf{V}_0 \,+\, \mathbf{V}_1\, t\,, \tag{7}$$

and has the first order of accuracy. Here $\mathbf{U}_0$ and $\mathbf{V}_0$ are the known initial nodal displacements and velocities, and the unknown nodal vector $\mathbf{V}_1$ can be expressed in terms of the unknown nodal vector $\mathbf{U}_1$ as follows:

$$\mathbf{V}_1 \,=\, \frac{1}{a_1}\mathbf{U}_1 \,-\, \frac{1}{a_1}\mathbf{V}_0\,. \tag{8}$$

Finally, the following system of algebraic equations is solved for the determination of $\mathbf{U}_1$

$$(\mathbf{M} \,+\, a_1\mathbf{C} \,+\, a_1^2\mathbf{K}\,)\mathbf{U}_1 \,=\, -\,a_1\mathbf{K}\,\mathbf{U}_0 \,+\, \mathbf{M}\,\mathbf{V}_0 \,+\, \mathbf{R}_1\,, \tag{9}$$

where

$$a_1 \,=\, \frac{m+2}{m+3}\Delta t\,, \tag{10}$$

$$\mathbf{R}_1 \,=\, \frac{(m+2)^2}{(m+3)\Delta t^{m+1}} \int_0^{\Delta t} \mathbf{R}(t) t^{m+1}\, dt\,. \tag{11}$$

The parameter m is responsible for the amount of numerical dissipation. After the calculation of $\mathbf{U}_1$ from Eq. (9), the values of displacements and velocities at the end of a time increment Δt are calculated using Eqs. (7) and (8) for $t = \Delta t$:

$$\mathbf{U}(\Delta t) \,=\, \mathbf{U}_0 \,+\, \mathbf{U}_1\, \Delta t\,, \qquad \mathbf{V}(\Delta t) \,=\, \mathbf{V}_0 \,+\, \mathbf{V}_1\, \Delta t\,. \tag{12}$$

The maximum numerical dissipation corresponds to $m = \infty$. For the case $m = \infty$, the parameter $a_1 = \Delta t$, and $\mathbf{R}_1$ should be calculated analytically; see Eqs. (11). However, in order to avoid the analytical calculation of $\mathbf{R}_1$ at $m = \infty$, a value $m \ge 15$ can be used in computations (the difference in numerical dissipation for $m = \infty$ and $m \ge 15$ is not very essential). Numerical examples show that the first-order accurate implicit TCG method suppresses spurious high-frequency oscillations for 10 time steps and retains good accuracy of a numerical solution at low modes. In order to have a numerical solution before and after the filtering stage at the same observation time, the first five uniform time increments are taken positive, and the last five uniform time increments are taken negative (the boundary conditions and external forces are zero during the filtering stage).

For the selection of minimum necessary amount of numerical dissipation for filtering spurious oscillations, a special calibration procedure was developed in [13]. The procedure was based on the analysis of spurious high-frequency oscillations for the 1-D impact problem for which the analytical solution is known (see [12, 13] for details). The following empirical formula for the selection of time increments for an implicit time-integration method with large numerical dissipation (the size of a time increment is related to the amount of numerical dissipation) is suggested in [12, 13] for 1-D elastodynamics problems:

$$\Delta t = \alpha(N_1)\frac{\Delta x \Omega_{0.1}(N)}{c}\,, \tag{13}$$

where $c = c_o = \sqrt{\frac{E}{\rho}}$ is the wave velocity; Δx is the size of a finite element; $\Omega_{0.1}(N)$ is the value of $\Omega = w\Delta t$ at which the spectral radius has the value 0.1 for the selected number N of time

increments; w is the frequency of vibration for a system with a single degree of freedom; $\Omega_{0.1}$ is used to scale spectral radii calculated at different numbers of time increments N; $\alpha(N_1)$ is the empirical coefficient depending on the time-integration method, the order of finite elements, and on the number N_1 of elements which are passed through by the wave front (this number can be expressed as $N_1 = \frac{cT}{\Delta x}$; see [12, 13]). For example, for the first-order implicit TCG method ($m = 15$), the following explicit expression is suggested in [13] for the coefficient $\alpha(N_1)$:

$$\alpha(\frac{cT}{\Delta x}) = a_1 \left(\frac{cT}{\Delta x}\right)^{a_2} . \tag{14}$$

The coefficients a_1 and a_2 for linear and quadratic elements with the consistent mass matrix are calculated in [13]. Using the calibration procedure described in [13], we found the following coefficients for linear elements with the averaged ($\gamma = 0.5$) mass matrix: $a_1 = 0.2942$ and $a_2 = 0.2104$ (see [14]); for linear elements with the standard consistent mass matrix: $a_1 = 0.2986$ and $a_2 = 0.3461$ (see [13]); for quadratic elements with the standard consistent mass matrix: $a_1 = 0.1948$ and $a_2 = 0.234$ (see [13]).

For the selection of the size of time increments for the filtering stage of 2-D and 3-D problems, the following modification of Eq. (13) can be used

$$\Delta t = \max_{i,j} \left[\alpha(\frac{c_i T}{\Delta x_j}) \frac{\Delta x_j}{c_i} \right] \Omega_{0.1}(N) \; = \; \max_{i,j} \left[\frac{\Delta x_j}{c_i} \right]^{1-a_2} a_1 \, T^{a_2} \, \Omega_{0.1}(N)$$
$$= \left[\frac{\max\limits_j \Delta x_j}{\min\limits_i c_i} \right]^{1-a_2} a_1 \, T^{a_2} \, \Omega_{0.1}(N) \; = \; \left[\frac{\Delta x_{max}}{c_2} \right]^{1-a_2} a_1 \, T^{a_2} \, \Omega_{0.1}(N) \, , \tag{15}$$

where $c_2 = \min\limits_i c_i$ $(i = 1, 2)$ is the minimum value between the velocities of the compressional wave $c_1 = \sqrt{\frac{\lambda+2\mu}{\rho}}$ and the shear wave $c_2 = \sqrt{\frac{\mu}{\rho}}$, $\Delta x_{max} = \max\limits_j \Delta x_j$ is the maximum dimension of finite elements along the axes x_j ($j = 1, 2$ for 2-D problems and $j = 1, 2, 3$ for 3-D problems). Eq. (15) is based on Eqs. (13) and (14) with the selection of the maximum size of a time increment with respect to the compressional and shear waves, and the dimensions of a finite element along the coordinate axes. For 2-D and 3-D uniform meshes with linear quadrilateral elements, we use the coefficients a_1 and a_2 obtained for the 1-D case; see Eq. (14). As shown in [12], Eq. (15) is the necessary condition for the selection of the amount of numerical dissipation in the multi-dimensional case.

REFERENCES

[1] H. P. Cherukuri. Dispersion analysis of numerical approximations to plane wave motions in an isotropic elastic solid. *Computational Mechanics*, 25(4):317–328, 2000.

[2] W. Dauksher and A. F. Emery. Solution of elastostatic and elastodynamic problems with chebyshev spectral finite elements. *Computer Methods in Applied Mechanics and Engineering*, 188(1):217–233, 2000.

[3] D. Gabriel, J. Plesek, R. Kolman, , and F. Vales. Dispersion of elastic waves in the contactimpact problem of a long cylinder. *Journal of Computational and Applied Mathematics*, 234:1930–1936, 2010.

[4] M. N. Guddati and B. Yue. Modified integration rules for reducing dispersion error in finite element method. *Computer Methods in Applied Mechanics and Engineering*, 193:275–287, 2004.

[5] S. Krenk. Dispersion-corrected explicit integration of the wave equation. *Computer Methods in Applied Mechanics and Engineering*, 191:975–987, 2001.

[6] K. J. Marfurt. Accuracy of finite difference and finite element modeling of the scalar and elastic wave equation. *Geophysics*, 49:533–549, 1984.

[7] R. Mullen and T. Belytschko. Dispersion analysis of finite element semidiscretizations of the two-dimensional wave equation. *International Journal for Numerical Methods in Engineering*, 18:11–29, 1982.

[8] G. Seriani and S. P. Oliveira. Optimal blended spectral-element operators for acoustic wave modeling. *Geophysics*, 72(5):95–106, 2007.

[9] B. Yue and M. N. Guddati. Dispersion-reducing finite elements for transient acoustics. *Journal of the Acoustical Society of America*, 118(4):2132–2141, 2005.

[10] F. I. Zyserman and P. M. Gauzellino. Dispersion analysis of a nonconforming finite element method for the three-dimensional scalar and elastic wave equations. *Finite Elements in Analysis and Design*, 41(13):1309–1326, 2005.

[11] A. V. Idesman. A new high-order accurate continuous galerkin method for linear elastodynamics problems. *Computational Mechanics*, 40:261–279, 2007.

[12] A. V. Idesman. Accurate time integration of linear elastodynamics problems. *Computer Modeling in Engineering and Sciences*, pages 1–38, 2011 (accepted).

[13] A. V. Idesman, H. Samajder, E. Aulisa, and P. Seshaiyer. Benchmark problems for wave propagation in elastic materials. *Computational Mechanics*, 43(6):797–814, 2009.

[14] A. V. Idesman, M. Schmidt, and J. R. Foley. Accurate finite element modeling of linear elastodynamics problems with the reduced dispersion error. *Computational Mechanics*, pages 1–18, 2011 (accepted, DOI 10.1007/s00466-010-0564-3).

[15] T. J. R Hughes. *The Finite Element Method: Linear Static and Dynamic Finite Element Analysis*. Prentice- Hall, Englewood Cliffs, NJ,, 1987.

[16] O. C. Zienkiewicz and R. L. Taylor. *The Finite Element Method*. Butterworth-Heinemann, Oxford, UK, 2000.

[17] A. Idesman, K. Subramanian, M. Schmidt, J. R. Foley, Y. Tu, and R. L. Sierakowski. Finite element simulation of wave propagation in an axisymmetric bar. *Journal of Sound and Vibration*, 329:2851–2872, 2010.

[18] G. M. Hulbert. Discontinuity-capturing operators for elastodynamics. *Computer Methods in Applied Mechanics and Engineering*, 96(3):409–426, 1992.

[19] G. M. Hulbert and T. J. R. Hughes. Space-time finite element methods for second-order hyperbolic equations. *Computer Methods in Applied Mechanics and Engineering*, 84(3):327–348, 1990.